

# Restratification Structure and Processes in the Irminger Sea

Miriam Frauke Sterl<sup>1</sup> and Marieke Femke de Jong<sup>2</sup>

<sup>1</sup>NIOZ Royal Netherlands Institute for Sea Research

<sup>2</sup>Royal Netherlands Institute for Sea Research NIOZ

November 24, 2022

## Abstract

The Irminger Sea is one of the few regions in the ocean where deep ( $> 1000$  m) convection occurs. Convection is followed by restratification during summer, when the stratification of the water column is reestablished and the convectively formed water is exported to the lower limb of the Atlantic Meridional Overturning Circulation (AMOC). We investigate the interannual variability and physical drivers of restratification in the upper 600 m of the central Irminger Sea using reanalysis data for the years 1993–2019. We find that there are distinctly different restratification processes in the upper 100 m of the water column (the upper layer) and the water below it (the lower layer). In the upper layer, the stratification is dominated by a strong seasonal cycle that matches the cycle of the surface heat flux. In 2010 and 2019, there were peaks in upper layer stratification, which could be related to strong atmospheric heat and freshwater fluxes. By contrast, in the lower layer the seasonal cycle is weaker and there is strong interannual variability. Restratification can continue for up to 5 months after the surface heat flux has become negative, indicating a role for lateral advection. The strength of the restratification is strongly correlated with the eddy kinetic energy in the eastern Irminger Sea. This suggests the lateral advection is driven by warm, saline eddies from the Irminger Current. In the future, surface warming and freshening of the Irminger Sea due to anthropogenic climate change are expected to increase stratification.



## Abstract

The Irminger Sea is one of the few regions in the ocean where deep ( $> 1000$  m) convection occurs. Convection is followed by restratification during summer, when the stratification of the water column is reestablished and the convectively formed water is exported to the lower limb of the Atlantic Meridional Overturning Circulation (AMOC). We investigate the interannual variability and physical drivers of restratification in the upper 600 m of the central Irminger Sea using reanalysis data for the years 1993–2019. We find that there are distinctly different restratification processes in the upper 100 m of the water column (the upper layer) and the water below it (the lower layer). In the upper layer, the stratification is dominated by a strong seasonal cycle that matches the cycle of the surface heat flux. In 2010 and 2019, there were peaks in upper layer stratification, which could be related to strong atmospheric heat and freshwater fluxes. By contrast, in the lower layer the seasonal cycle is weaker and there is strong interannual variability. Restratification can continue for up to 5 months after the surface heat flux has become negative, indicating a role for lateral advection. The strength of the restratification is strongly correlated with the eddy kinetic energy in the eastern Irminger Sea. This suggests the lateral advection is driven by warm, saline eddies from the Irminger Current. In the future, surface warming and freshening of the Irminger Sea due to anthropogenic climate change are expected to increase stratification.

## Plain Language Summary

In the Irminger Sea, cold winters can cause the surface ocean to cool enough that they start mixing downward. The mixing can continue for months and eventually form a dense water mass with uniform properties of more than 1 km deep. This process is called deep convection. During summer, the dense water gets exported to large depths, and the water column will go back to its original structure with lighter waters over denser waters. This is called restratification. The formation and export of dense waters in the Irminger Sea plays an important role in the global ocean circulation. Here we study what drives the restratification in the central Irminger Sea, and how it varies in time. We find that in the surface layer (0–100 m) the restratification is driven by heating from the atmosphere, which warms the surface waters and makes them lighter. Additionally, rainfall or ice melt which make the surface waters fresher contribute to restratification. Below the surface layer, restratification happens through transport of warm and saline waters from the eastern Irminger Sea. With rising ocean temperatures due to climate change, the Irminger Sea might see more restratification and less deep convection in the future.

## 1 Introduction

The Atlantic Meridional Overturning Circulation (AMOC) plays an important role in the global climate system (e.g. Pérez et al., 2013; McCarthy et al., 2017; Fox-Kemper et al., 2021). In the Atlantic upper ocean, warm and saline waters are transported northward in the AMOC’s upper limb from the equator to high latitudes, where wintertime deep convection transforms them into colder and denser waters. These dense waters can spread to the AMOC’s lower limb in the deep ocean, where they remain isolated from the atmosphere for hundreds to thousands of years. Thus the AMOC has an important effect on the ocean’s uptake and storage of heat and anthropogenic  $\text{CO}_2$  from the atmosphere (Fröb et al., 2016; Brown et al., 2021). Deep convection can theoretically be described as a three-phase process (Jones & Marshall, 1997; Marshall & Schott, 1999; Gelderloos et al., 2011; de Jong et al., 2018). It starts with the preconditioning phase, which consists of a large-scale (order of 100 km) cyclonic gyre circulation with ‘doming’ isopycnals, bringing weakly stratified waters of the interior close to the surface. The second phase is the deep convection phase, during which strong winter buoyancy loss gradually deepens the mixed layer, forming a large and deep ‘mixed patch’ or ‘convective patch’

64 with a diameter in the order of 100 km and a depth in the order of 1 km. The deep con-  
65 vection is followed by the restratification phase which occurs after winter, in spring and  
66 summer, on a time scale of weeks to months. During this phase the stratification of the  
67 convective patch is reestablished by surface buoyancy gain and by lateral exchange be-  
68 tween the convective patch and its stratified environment. The restratification determines  
69 the stratification at the start of the next deep convection phase and thus affects precon-  
70 ditioning. There are only a few areas in the world's oceans where deep convection (more  
71 than 1 km) occurs. Two important deep convection regions are the Labrador Sea (e.g.  
72 Lilly et al., 1999; Lazier et al., 2002; Straneo, 2006a; Yashayaev & Loder, 2017) and the  
73 Irminger Sea (e.g. Pickart et al., 2003; De Jong et al., 2012; de Jong & de Steur, 2016;  
74 Piron et al., 2016; de Jong et al., 2018), located west and east of Greenland, respectively.  
75 The convectively formed dense waters in these basins can spread to the seas' perimeter  
76 and enter the lower limb of the AMOC (Straneo, 2006b; Katsman et al., 2018; Georgiou  
77 et al., 2019; Le Bras et al., 2020).

78 Multiple studies have addressed the restratification phase in the Labrador Sea. It  
79 was found that there is interannual variability in the deep convection as well as in the  
80 restratification in the Labrador Sea (e.g. Lazier et al., 2002; Straneo, 2006a; de Jong et  
81 al., 2016). Straneo (2006a) found that there are distinct temporal behaviours in the sur-  
82 face layer between 0–200 m and the lower layer between 200–1300 m in the Labrador Sea  
83 interior. The surface layer properties follow a strong seasonal cycle, whereas the lower  
84 layer properties show strong interannual variability. Moreover, the surface layer fresh-  
85 ens during summer and becomes more saline during winter; these signs in the seasonal  
86 cycle are reversed for the lower layer. Many studies have focused on the lateral exchange  
87 between the interior, where deep convection occurs, and the buoyant cyclonic boundary  
88 current in the Labrador Sea. Katsman et al. (2004) and Gelderloos et al. (2011) found  
89 that Irminger Rings (IRs) shed by the West Greenland Current (WGC) near the west  
90 coast of Greenland are an important contributor to restratification. Observations from  
91 Lilly et al. (1999), Hátún et al. (2007) and de Jong et al. (2014) show that IRs consist  
92 of a warm and saline core topped by a colder and fresher surface layer. This can be re-  
93 lated to the structure of the WGC, which consists of warm and saline Irminger Sea Wa-  
94 ter (ISW) below colder and fresher polar waters (Cuney et al., 2002). The IR vertical struc-  
95 ture contributes to the distinct behaviours in the upper and lower layer in the interior  
96 Labrador Sea found by Straneo (2006a).

97 Deep convection also occurs in the cyclonic Irminger Gyre (Våge et al., 2011; De Jong  
98 et al., 2012; de Jong & de Steur, 2016; de Jong et al., 2018). Recent studies by Lozier  
99 et al. (2019), Petit et al. (2020) and Li et al. (2021) found that deep convection in the  
100 Irminger Sea is a major contributor to overturning in the North Atlantic subpolar gyre.  
101 Moreover, the Irminger Sea is found to be an important region for anthropogenic car-  
102 bon uptake (Fröb et al., 2016). While the relation between surface buoyancy forcing and  
103 Irminger Sea deep convection has been described (De Jong et al., 2012; de Jong & de  
104 Steur, 2016; de Jong et al., 2018), the relation to changes in stratification is less explored.  
105 Since deep convection is predicted to weaken under climate change as a result of increas-  
106 ing stratification, it is important to study processes that contribute to stratification in  
107 the Irminger Sea. Therefore, this study aims to provide a description of the vertical struc-  
108 ture and temporal variability of restratification in the Irminger Sea, as well as of the phys-  
109 ical processes that contribute to it.

110 This paper is organised as follows: in Section 2, the data sets and methods used  
111 for the study are introduced. We employ an ocean reanalysis, validated against local moor-  
112 ing data, as well as surface flux data from atmospheric reanalysis. In Section 3, we de-  
113 scribe the general hydrographic properties in the Irminger Sea and the interannual vari-  
114 ability in stratification; moreover, we investigate the physical processes, such as surface  
115 forcing and eddy processes, that contribute to restratification. Finally, a summary and  
116 discussion of the results are presented in Section 4.

## 2 Data and Methods

### 2.1 Data

We used the GLORYS12V1 global ocean physics reanalysis from the Copernicus Marine Environment Monitoring Service (CMEMS; Fernandez & Lellouche, 2018) to investigate hydrographic variability in the Irminger Sea. GLORYS12V1 uses the NEMO model component (Madec, 2016) and is forced at the surface by ECMWF ERA-Interim reanalysis from 1993–2017, which was replaced by ERA5 reanalysis for recent years. For this study, we used the monthly mean data for the period from January 1993 until December 2019. The data set has a spatial resolution of  $1/12^\circ$  and has 50 vertical levels, with vertical intervals of 1 m at the surface increasing to 450 m at the bottom. The variables obtained from the data set are the potential temperature (`thetao`), practical salinity (`so`), eastward and northward ocean current velocity (`uo` and `vo`), and mixed layer depth (`m1otst`). The mixed layer depth (henceforth abbreviated as MLD) in CMEMS is defined as the depth where the density difference compared to a reference level is  $0.01 \text{ kg/m}^3$  (Madec, 2016, p. 246). The TEOS-10 software was used to recompute practical salinity to absolute salinity  $S_A$ , and potential temperature to conservative temperature  $\Theta$  (McDougall & Barker, 2011). From these properties, the potential density anomaly referenced to the surface,  $\sigma_0$ , could then be computed. From now on, unless explicitly stated otherwise, every mention of salinity, temperature, and density from the CMEMS data will refer to  $S_A$ ,  $\Theta$ , and  $\sigma_0$ , respectively. The current velocities were used to compute eddy kinetic energy (EKE), defined as

$$\text{EKE} = \frac{1}{2} \left[ (u - \bar{u})^2 + (v - \bar{v})^2 \right], \quad (1)$$

where  $\bar{u}$  and  $\bar{v}$  are the time-mean zonal and meridional velocity components over the whole time series.

To validate the CMEMS data, it was compared to data from the Long-term Ocean Circulation Observations (LOCO) mooring, which was located at  $39.5^\circ\text{W}$ ,  $59.2^\circ\text{N}$  (Figure 1) from September 2003 until June 2018. The processed data from September 2003 until July 2015 as published by De Jong et al. (2012), de Jong and de Steur (2016) and de Jong et al. (2018) were used. The LOCO data is not assimilated in the CMEMS reanalysis and therefore provides an independent comparison of the reanalysis data with observations. For the comparison, the original daily resolution of the LOCO data was reduced to monthly means. This time series is compared to the CMEMS data interpolated at the LOCO mooring location. The comparison between the two data sets is described in the Supplementary Material.

To study atmospheric fluxes at the ocean surface, we used the ERA5 reanalysis from the Copernicus Climate Change Service (C3S) Climate Data Store (CDS) (Hersbach et al., 2020). The monthly averaged data at the surface was selected for January 1993 until December 2019. The data set has a horizontal resolution of  $0.25^\circ$ . For freshwater fluxes the evaporation (`e`) and total precipitation (`tp`) were studied; the sum of these two yields the net atmospheric freshwater flux  $\mathcal{F}$ . For heat fluxes the surface net solar radiation (`ssr`), surface net thermal radiation (`str`), surface latent heat flux (`slhf`), and surface sensible heat flux (`sshf`) were used to obtain the net atmospheric heat flux  $Q$ .

### 2.2 Methods

#### 2.2.1 Defining the Deep Convection Area

Because the aim of this study is to describe restratification after deep convection, we needed to identify the area within the Irminger Sea where deep convection occurs. We focused on the southwestern part of the Irminger Sea, where the centre of the cyclonic Irminger Gyre is located. Out of the 27 years within the CMEMS data set, there are 28 winter months in which MLDs of more than 1 km deep occurred in this region.

165 The MLD field was averaged over these months and the result is shown in Figure 1. The  
 166 650 m contour of this MLD field smoothed with a Gaussian filter ( $\sigma = 5$  grid cells =  
 167  $5/12^\circ$ ) was chosen as the boundary of the deep convection area, which we will abbreviate  
 168 as DCA. The data from the CMEMS and ERA5 reanalyses were averaged over the  
 169 DCA to get time series of surface freshwater and heat fluxes, MLD, and salinity, tem-  
 170 perature and density profiles in the DCA.

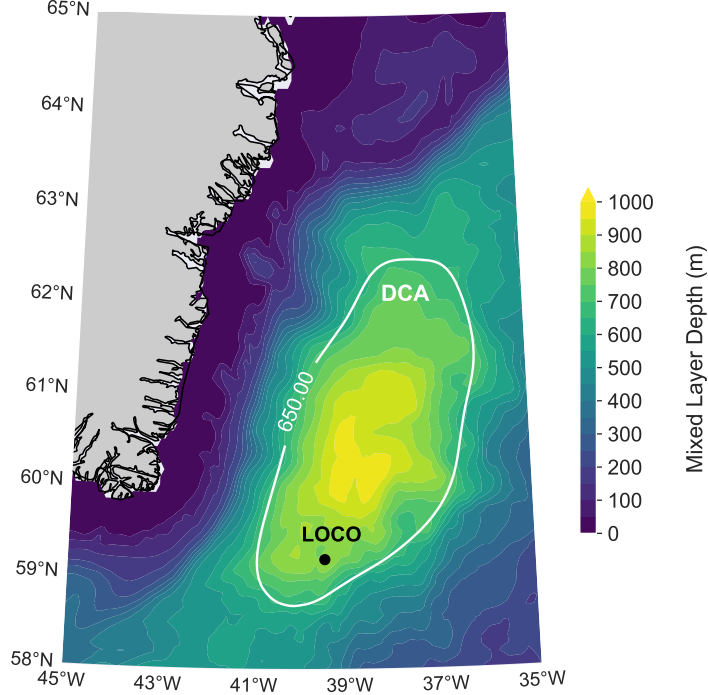


**Figure 1.** The mixed layer depth (MLD) field averaged over the months from the monthly 1993–2019 CMEMS data set in which the maximum MLD within the region  $[45^\circ\text{W}, 35^\circ\text{W}] \times [58^\circ\text{N}, 65^\circ\text{N}]$  exceeds 1000 m. In white, the 650 m contour of this MLD field smoothed with a Gaussian filter ( $\sigma = 5$  grid cells) is shown, representing the boundary of the Deep Convection Area (DCA). The black dot shows the location of the LOCO mooring used for data validation.

### 171 **2.2.2 Quantifying Stratification and Restratification**

172 As a quantitative measure of the stratification of the water column between  $z =$   
 173  $-h_1$  and  $z = -h_2$  (where  $0 \leq h_1 < h_2$ ), we used the stratification index (SI), defined  
 174 as the integral of the potential density gradient times depth:

$$175 \text{SI} = \int_{-h_2}^{-h_1} \frac{\partial \sigma}{\partial z} z \, dz, \quad (2)$$

176 with units of  $\text{kg}/\text{m}^2$ . Partial integration of Equation (2) yields an expression of the SI  
 177 in terms of the density profile  $\sigma(z)$  (rather than the density *gradient* profile):

$$178 \text{SI} = -h_1 \sigma(-h_1) + h_2 \sigma(-h_2) - \int_{-h_2}^{-h_1} \sigma(z) \, dz. \quad (3)$$

179 The SI is the amount of buoyancy that must be removed in order for the water column  
 to mix down from depth  $-h_1$  to depth  $-h_2$  with subsequent uniform density. A stratified  
 layer has a positive SI, a perfectly mixed layer has an SI of zero, and an unstable

180 layer about to overturn has a negative SI. The SI has been used as a measure for strat-  
 181 ification in various Mediterranean studies, where it is usually defined with a factor  $g/\rho_0$   
 182 so that it is the integral of the Brunt-Väisälä frequency (e.g. Herrmann et al., 2010; L'Hévéder  
 183 et al., 2013; Somot et al., 2018; Margirier et al., 2020). The partial integration Equation  
 184 (3) multiplied by  $-1$  has also been used in North Atlantic Studies; Bailey et al. (2005)  
 185 referred to it as the integrated buoyancy anomaly, and Frajka-Williams et al. (2014) called  
 186 it the Convection Resistance.

187 To study the influence of temperature and salinity on the stratification, two ad-  
 188 ditional values of the SI were computed:  $SI_T$  and  $SI_S$ , which only consider the contri-  
 189 bution of temperature and salinity to stratification, respectively. This was done by us-  
 190 ing the linear approximation for the density of seawater (Dijkstra, 2008):

$$\rho = \rho_0 [1 - \alpha (\Theta - \Theta_0) + \beta (S_A - S_{A,0})], \quad (4)$$

191 where  $\Theta_0$  and  $S_{A,0}$  are a reference temperature and salinity and  $\rho_0 = \rho(\Theta_0, S_{A,0})$  is  
 192 a reference in-situ density. Furthermore,  $\alpha = -\partial\rho/\partial\Theta$  is the thermal expansion coef-  
 193 ficient with units  $1/K$ , and  $\beta = \partial\rho/\partial S_A$  is the saline contraction coefficient in  $kg/g$ .  
 194 Based on Equation (4), we can view  $-\alpha\Theta$  as a first approximation of the temperature  
 195 contribution to density, and similarly  $\beta S_A$  as the salinity contribution. Hence, replac-  
 196 ing  $\sigma$  in Equation (3) by  $-\alpha\Theta$  and  $\beta S_A$ , respectively, yields an approximation of the tem-  
 197 perature and salinity contribution to stratification, which we denote as  $SI_T$  and  $SI_S$ . Note  
 198 that  $-\alpha\Theta$  and  $\beta S_A$  are unitless, so that the stratification contributions  $SI_T$  and  $SI_S$  are  
 199 given in m instead of  $kg/m^2$ . From the time series of salinity, temperature and density  
 200 profiles averaged over the DCA, monthly values of the SI,  $SI_T$  and  $SI_S$  were computed.

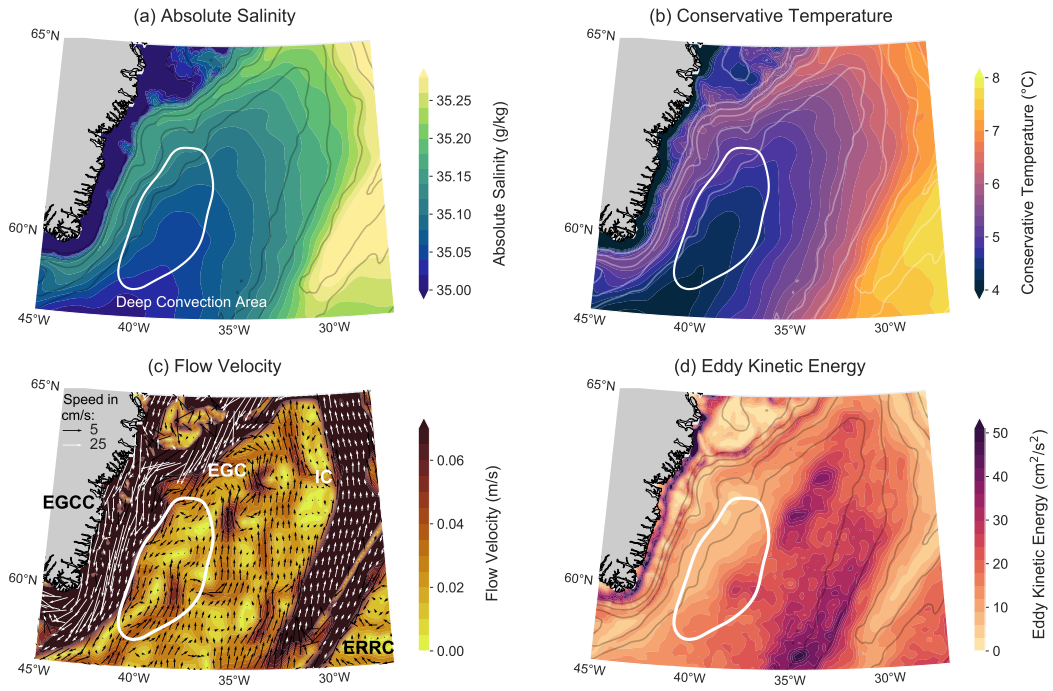
201 Using the SI, a quantitative measure for restratification could be created as well.  
 202 The restratification in a certain year was defined to be the increase in SI from the min-  
 203 imum in winter to the maximum in summer. Thus the monthly time series of the SI could  
 204 be used to compute annual time series of restratification.

### 3 Results

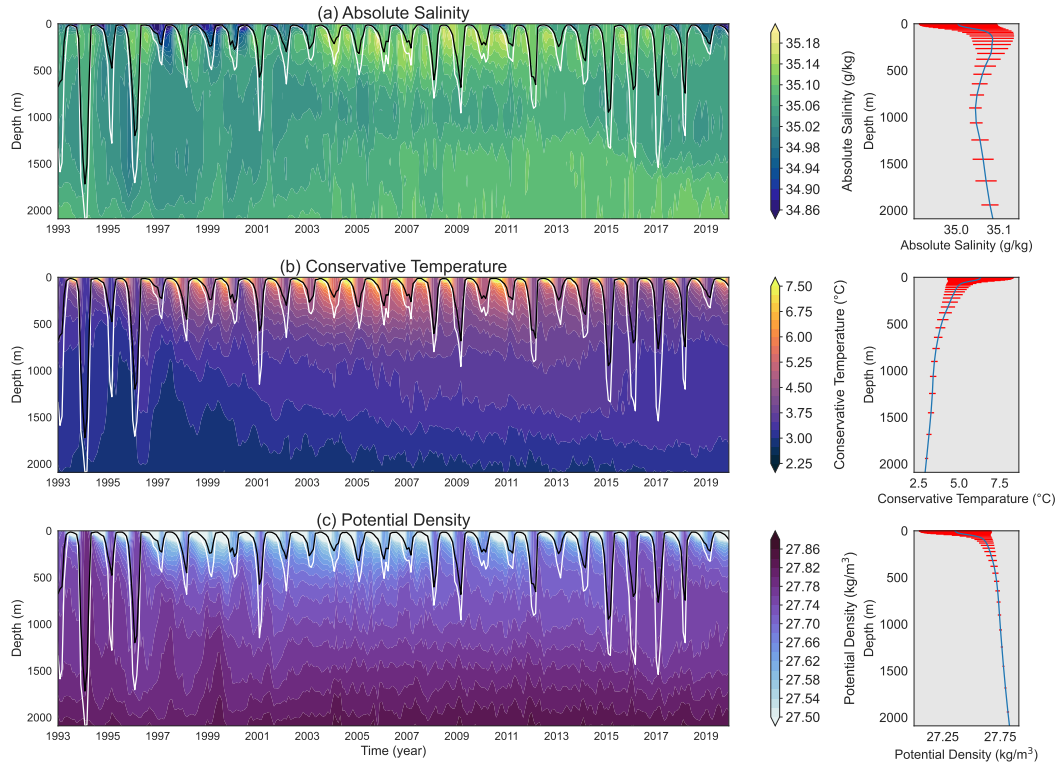
#### 3.1 The Deep Convection Area

Figure 2 shows maps of the time-mean hydrographic properties in the Irminger Sea. All of these properties are depth-averaged over the upper 600 m, where the variability in density related to convection and restratification is strongest (Figure 3). From Figure 2 we can identify the main currents and their characteristics. On the eastern side of the Irminger Sea we find the northward-flowing Irminger Current (IC) transporting warm and saline water originating from the North Atlantic Current (de Jong et al., 2020; Fried & Jong, 2022). The IC follows the bathymetry, so around 65°N, it veers west and continues southward along the East Greenland Shelf. Alongside this part of the IC we find two currents of Arctic origin, which are thus fresher and colder: the East Greenland Current (EGC) along the shelfbreak and the East Greenland Coastal Current (EGCC) on the inner shelf (e.g. Le Bras et al., 2018; Duyck & De Jong, 2021). The EKE in the Irminger Sea is highest in the IC, in the EGCC and to the northeast of the DCA. These regions are in agreement with the strong EKE regions that were derived from surface drifter data by Fratantoni (2001) and from satellite altimetry data by Volkov (2005) and Fan et al. (2013). Eddies observed in the central Irminger Sea travel westward and have a warm and saline core, which suggests that they are shed by the IC (Fan et al., 2013).

To study the interannual variability and vertical structure of hydrographic properties in the DCA, we consider the full 1993–2019 time series of spatially averaged profiles of DCA salinity, temperature and density (Figure 3). The mean and maximum MLD over the DCA are also shown. The temperature and density have monotonously stratified structures, with warm, buoyant layers above cold, dense ones. By contrast, salinity has a mid-depth minimum in the layer between 500 and 1500 m, which is the signature of convectively formed water. From the evolution of the MLD we see that there is strong interannual variability in the convection strength. There is also interannual variability in stratification: some years have much weaker vertical density gradients than other years. In the early 1990s, cold and stormy winters forced the deepest mixed layers of the time series (Våge et al., 2011), which led to weak vertical density gradients and outcropping of isopycnals. In the 2000s, mixed layers were shallower, and the DCA was more stratified. From 2015 until 2018, the MLD increased again, resulting in a thickening of deep cold and dense layers and thus a decrease in stratification. The largest temporal fluctuations in hydrographic properties are found in the upper 600 m of the water column (right column of Figure 3), on which we will focus. Below this depth the temporal variations in density become very small; at 600 m the standard deviation in density is only 7.3% of that at the surface.



**Figure 2.** The 1993–2019 mean from the CMEMS reanalysis of the (a) absolute salinity, (b) conservative temperature, (c) flow velocity and (d) eddy kinetic energy in the Irminger Sea, averaged over the upper 600 m of the ocean. The white contour indicates the boundary of the Deep Convection Area. In panels (a), (b) and (d), smoothed contours of the bathymetry between 500 m and 2500 m are shown at 500 m intervals. In panel (c), velocity direction and magnitude are indicated by vectors. Velocities smaller than 0.07 m/s are indicated by black arrows, larger velocities by white arrows. The black and white vectors have different scalings, as shown by the reference vectors in the top right of the panel. In this panel the different currents are indicated: EGCC = East Greenland Coastal Current; EGC = East Greenland Current; IC = Irminger Current; ERRC = East Reykjanes Ridge Current.



**Figure 3.** The temporal evolution of profiles of (a) absolute salinity, (b) conservative temperature and (c) potential density from the CMEMS reanalysis averaged over the Deep Convection Area (DCA). The mixed layer depth averaged over the DCA is shown in black; the maximum mixed layer depth reached within the DCA is shown in white. The panels on the right show the 1993–2019 time-mean (blue curve) and standard deviations (red bars) of each variable.

241

### 3.2 Structure and Variability of Restratification

242

243

244

245

246

247

248

249

250

251

252

253

254

255

256

257

258

259

260

261

262

263

264

265

266

267

268

269

To see how properties within the DCA generally vary throughout the year, we composed climatologies of the salinity, temperature and density profiles in the upper 600 m of the DCA (Figure 4). A seasonal cycle consisting of deepening convection in autumn and winter, followed by restratification in spring and summer, is clearly visible in all three variables. The deepest mixed layers are typically reached in February through April (although a few years with shallower convection imprint as a slight non-zero vertical gradient in the climatology). Restratification sets in in April and May, with the halocline, thermocline and pycnocline steepening through to August (for temperature and density) and September (for salinity). The uppermost 30–50 m of the water column is typically characterised by a wind-mixed layer (Sampe & Xie, 2007). The salinity climatology (Figure 4a) shows different behaviour in the upper and lower parts of the water column. In summer, the surface layer freshens, likely through precipitation and freshwater from the Greenland shelf (Duyck & De Jong, 2021; Duyck et al., 2022). The deeper part of the water column is dominated by lateral exchange with the perimeter of the Irminger Sea, where salinity is generally higher than in the DCA (Figure 2a). In winter, convection homogenises the salinity over the upper and lower layer, making the former saltier and the latter fresher. The temperature and density climatologies (Figure 4b,c) exhibit the same sign in change over the upper 600 m, but a difference in timing and magnitude in restratification in the upper and lower layer can still be observed. In the upper layer, the increase in temperature is much stronger and maximum temperatures are reached in August. This is likely the effect of heat gain through surface fluxes (Figure 5). In the lower layer, the temperature gradient remains significantly weaker and warming continues until November, as is expected from warming by lateral exchange with somewhat warmer waters (Figure 2b). The net effect of temperature and salinity is a strong increase in stable density gradient in the upper layer during summer and a weaker, delayed increase below (Figure 4c). Given the different behaviour in restratification in the upper layer down to 100 m and the lower layer below (down to 600 m), we will study the interannual variability in these layers separately.

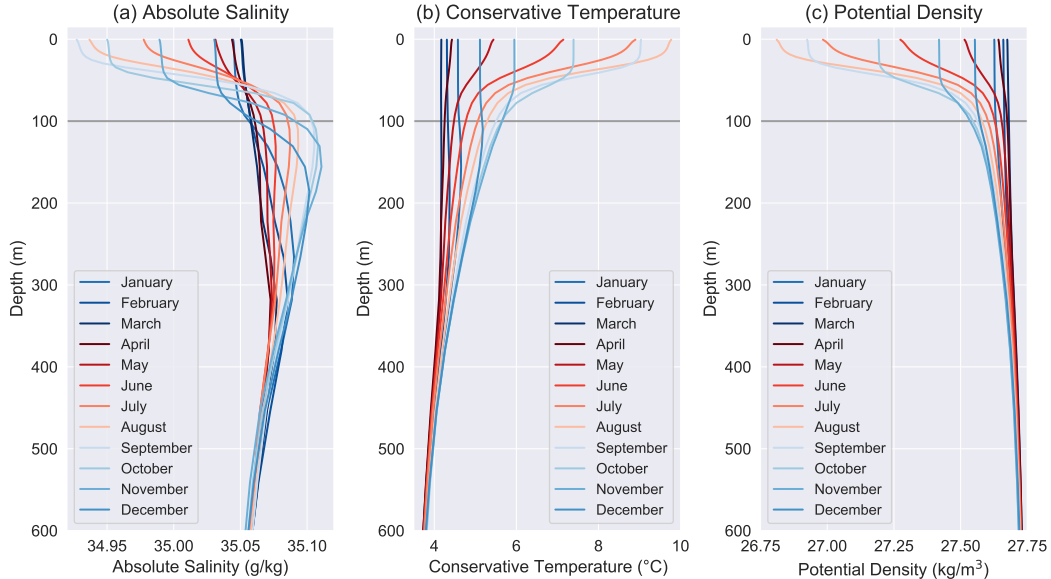


**Figure 4.** Climatologies of the (a) absolute salinity, (b) conservative temperature and (c) potential density profiles averaged over the Deep Convection Area, from the monthly 1993–2019 CMEMS reanalysis.

270 The stratification index of the two layers is shown in Figure 5, together with the  
 271 climatology of the MLD, the net surface heat flux and the net surface freshwater flux.  
 272 The SI climatology shows the difference in timing described above. Additionally, the lower  
 273 layer SI has a larger standard deviation in the lower layer, indicating stronger interan-  
 274 nual variability. Increasing upper layer SI matches with periods of surface heating and  
 275 decreasing upper layer SI with surface cooling. Timing in lower layer SI matches with  
 276 the MLD as expected. The net surface freshwater flux is highly variable, but generally  
 277 is higher in summer than in winter, which can add to the summer freshening of the up-  
 278 per layer. This is discussed further in relation to the interannual variability in Section  
 279 3.3.

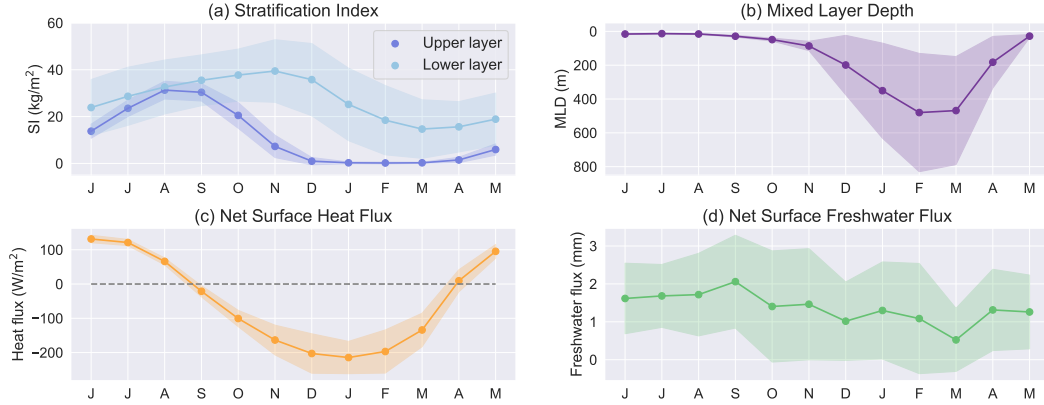


**Figure 5.** Climatologies of the (a) stratification index in the upper and lower layer, (b) mixed layer depth, (c) net surface heat flux and (d) net surface freshwater flux averaged over the Deep Convection Area. The data of (a) and (b) are from the monthly 1993–2019 CMEMS reanalysis, the data of (c) and (d) are from the monthly 1993–2019 ERA5 reanalysis. The shaded areas indicate the standard deviations.

280 The time series of SI and restratification from 1993 to 2019 (Figure 6) show the  
 281 difference in interannual variability in the upper, lower and total (upper+lower) layer.  
 282 The upper layer stratification is dominated by the seasonal cycle, with very little inter-  
 283 annual variability in either SI or restratification. Two years (2010 and 2019) stand out  
 284 as having higher summer maxima and we will come back to these in Section 3.3.2. In  
 285 the lower layer interannual variability dominates over seasonality. Unlike in the upper  
 286 layer, where the SI is set to zero each winter, the lower layer has a memory of stratifi-  
 287 cation and mixing over previous years. The stratification over the total layer (from 0–  
 288 600 m) is the superposition of the strong seasonal cycle in the upper layer and the in-  
 289 terannual variability in the lower layer.

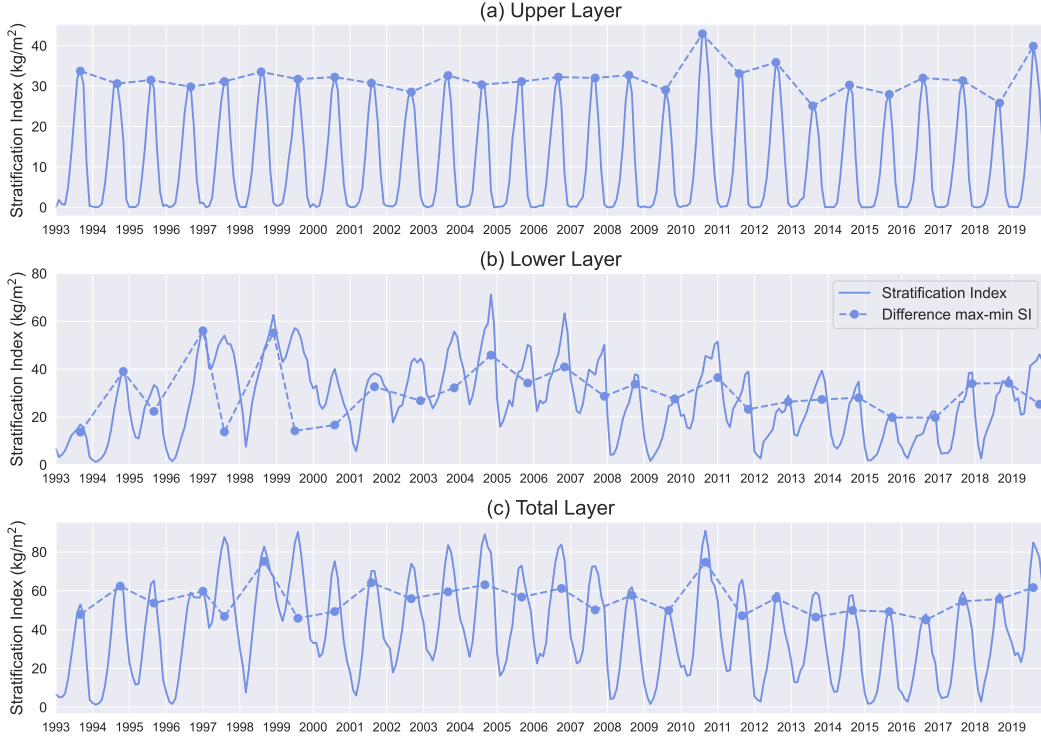


**Figure 6.** The stratification index (SI) time series in the Deep Convection Area for (a) the upper layer from 0–100 m, (b) the lower layer from 100–600 m, and (c) the total (upper+lower) layer from 0–600 m. The dashed line shows the annual values of the restratification, defined as the increase in SI from the minimum in winter to the maximum in summer.

290 **3.3 Physical Processes Contributing to Restratification**

291 **3.3.1 Role of Salinity and Temperature in Restratification**

292 The climatology in Figure 4 suggested there are different roles for temperature and  
 293 salinity in restratification. To study these further, we investigate time series of the  $SI_T$   
 294 and  $SI_S$  as introduced in Section 2.2.2 (Figure 7). In the upper layer, the  $SI_T$  and  $SI_S$   
 295 both follow a strong seasonal cycle. Values are slightly negative in winter indicating un-  
 296 stable stratification during deep convection and positive for the remainder of the year  
 297 due to higher temperatures and lower salinities. In the lower layer the  $SI_S$  is always neg-  
 298 ative, indicating the destabilising effect of salinity (saline water over fresher water) seen  
 299 also in Figure 4a. Despite the stable, fresh upper layer, the effect of salinity over the to-  
 300 tal 0–600 m layer is destabilising. Since the temperature exhibits the same sign gradi-  
 301 ent over both layers, the effect of temperature is always stabilising except during some  
 302 winter months with deep mixed layers (cf. Figure 3). In the lower layer, temperature and  
 303 salinity co-vary as the restratifying waters from the perimeter are warm and saline. This  
 304 is not necessarily so for the upper layer, where heat and freshwater fluxes can vary in-  
 305 dependently. Even so, the correlation between the variability in  $SI_S$  and  $SI_T$  is quite strong.  
 306 From the yearly restratification contributions in Figure 7 it can be seen that the restrat-  
 307 ification contribution of temperature (light dashed line) is always larger than that of salin-  
 308 ity (dark dashed line) in absolute value.

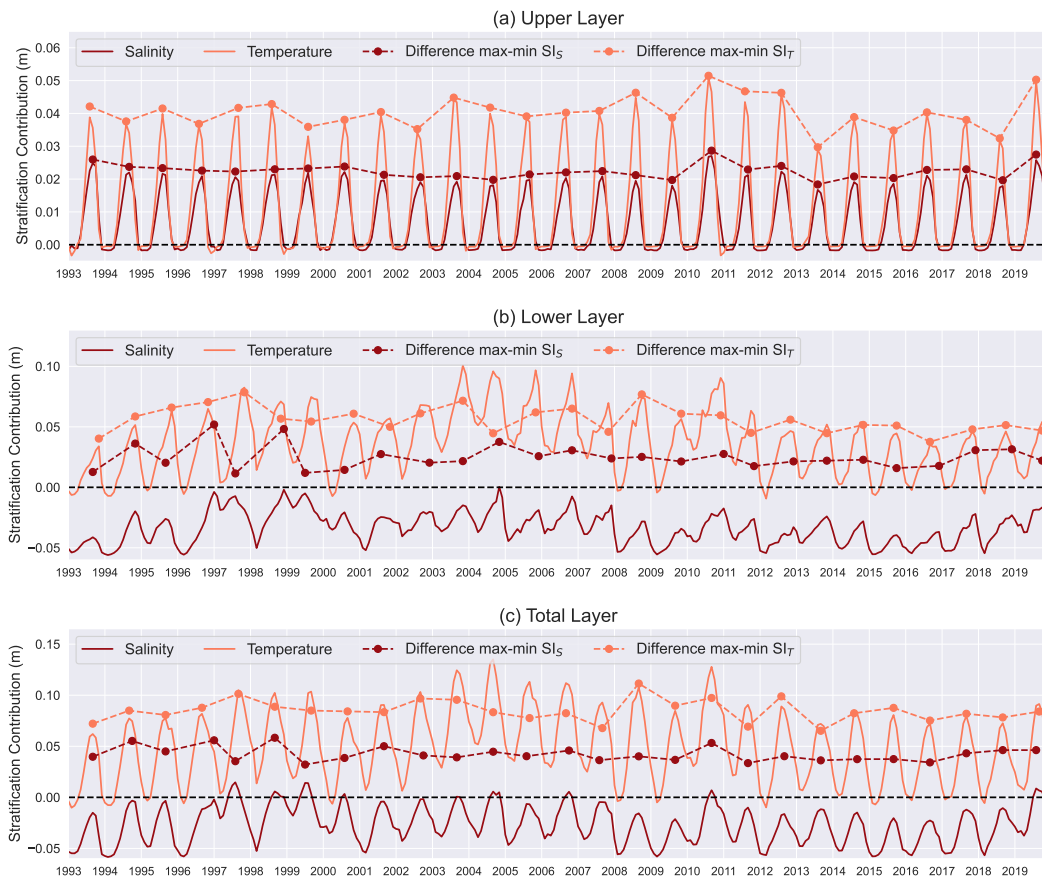


**Figure 7.** The stratification contribution of salinity and temperature in the Deep Convection Area for (a) the upper layer from 0–100 m, (b) the lower layer from 100–600 m, and (c) the total water layer from 0–600 m. The dashed lines show the annual values of the restratification, defined as the increase in stratification contribution from the minimum in winter to the maximum in summer.

309

### 3.3.2 Role of Surface Fluxes and Lateral Fluxes in Restratification

310

311

312

313

314

315

316

317

318

319

320

321

322

323

324

The climatology from Figure 5 suggested a relation between upper layer stratification and surface fluxes. Therefore we investigate interannual variability in surface heat and freshwater fluxes over the period of restratification, from the winter minimum  $SI$  in the upper layer to the next summer maximum of each year. Figure 8 shows the spring/summer accumulated atmospheric freshwater and heat fluxes together with the annual upper layer restratification. The restratification is not significantly correlated with either the surface freshwater flux nor with the heat flux separately. However, in years when both are stronger than average, they may reinforce each other. This appears to be the cases for the years with the highest restratification values, 2010 and 2019. Both years were characterised by above-average freshwater and heat gain during the restratification period, with the high freshwater gain mainly due to low evaporation (not shown here). The presence of a fresh surface layer, which already increased stratification, restricted warming by the high heat flux to a layer, resulting in higher temperatures and very high stratification by the end of summer. The reverse does not appear to be true; years with below-average heat and freshwater fluxes do not exhibit much weaker restratification.

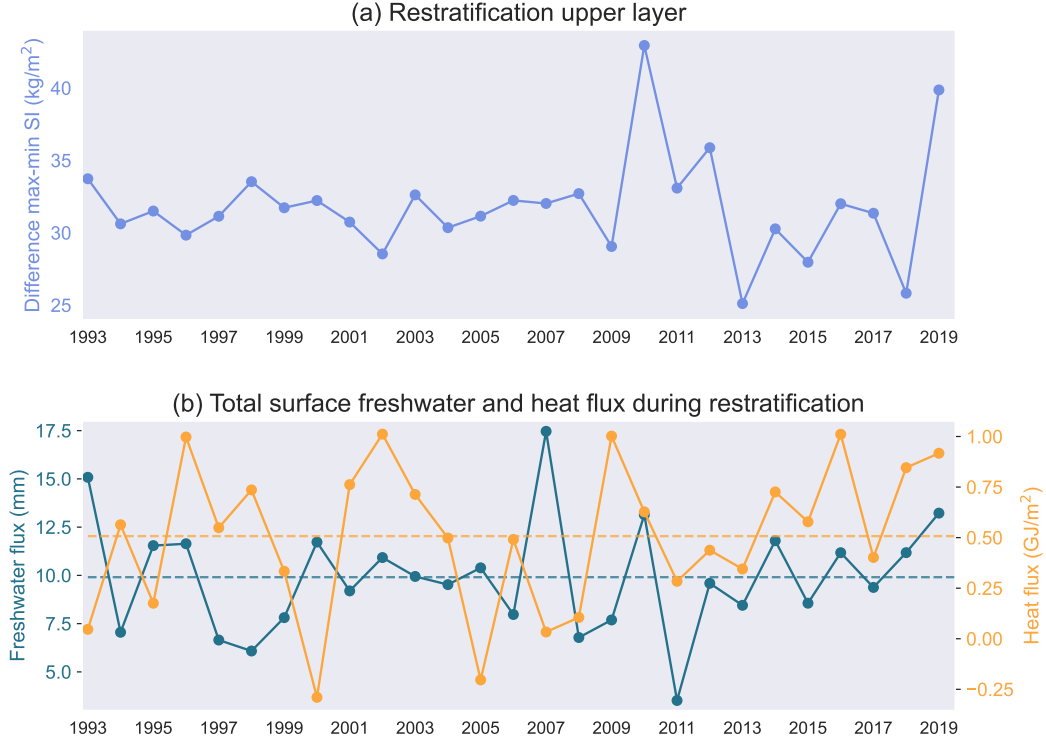


**Figure 8.** Annual time series of (a) restratification and (b) total accumulated surface freshwater and heat flux during the restratification period in the upper layer over the Deep Convection Area. The restratification period starts in the month after the occurrence of the minimum winter stratification index (SI) and ends in the month of the next maximum SI in the upper layer. The dashed horizontal lines show the time-mean values of the depicted time series.

325 In the lower layer, as opposed to the upper layer, there is strong interannual variability in both the summer maximum SI and the winter minimum SI (Figure 6b). In winter, the stratification in the lower layer is directly affected by the MLD (significant correlation of  $-0.68$  at a 95% significance level). Figure 9a shows the annual restratification in the lower layer together with the maximum MLD in the preceding winter. Years with high maximum stratification, such as 2004 and 2006, were preceded by winters with shallow mixed layers (MLD  $< 600$  m) so that some stratification remained at the end of winter. By contrast, years in which the maximum stratification was low, e.g. 2009 and 2015 (Figure 6b), were preceded by mixed layers of more than 750 m deep. However, there is no significant correlation between the MLD and the restratification in the lower layer. On the longer time scales (order of 10 years) they are correlated, but this may also be caused by both processes responding to changes in North Atlantic Oscillation phases.

337 During spring and summer the lower layer is isolated from the upper layer, so the lower layer restratification is less affected by surface fluxes and more by lateral advection of buoyant water from the perimeter of the Irminger Sea. Since this advection must cross the streamlines of the Irminger Gyre to enter the DCA, it is likely facilitated by eddies. This appears to be supported by the relation between the time series of lower layer restratification and mean surface EKE during restratification (Figure 9b; significantly correlated at  $r = 0.66$ ). The EKE time series is averaged over the area of the WOCE AR7E line (Koltermann et al., 2011) that lies east of the eastern DCA boundary between 315 and 700 km (Figures 9c and d), where the highest EKE values are found.

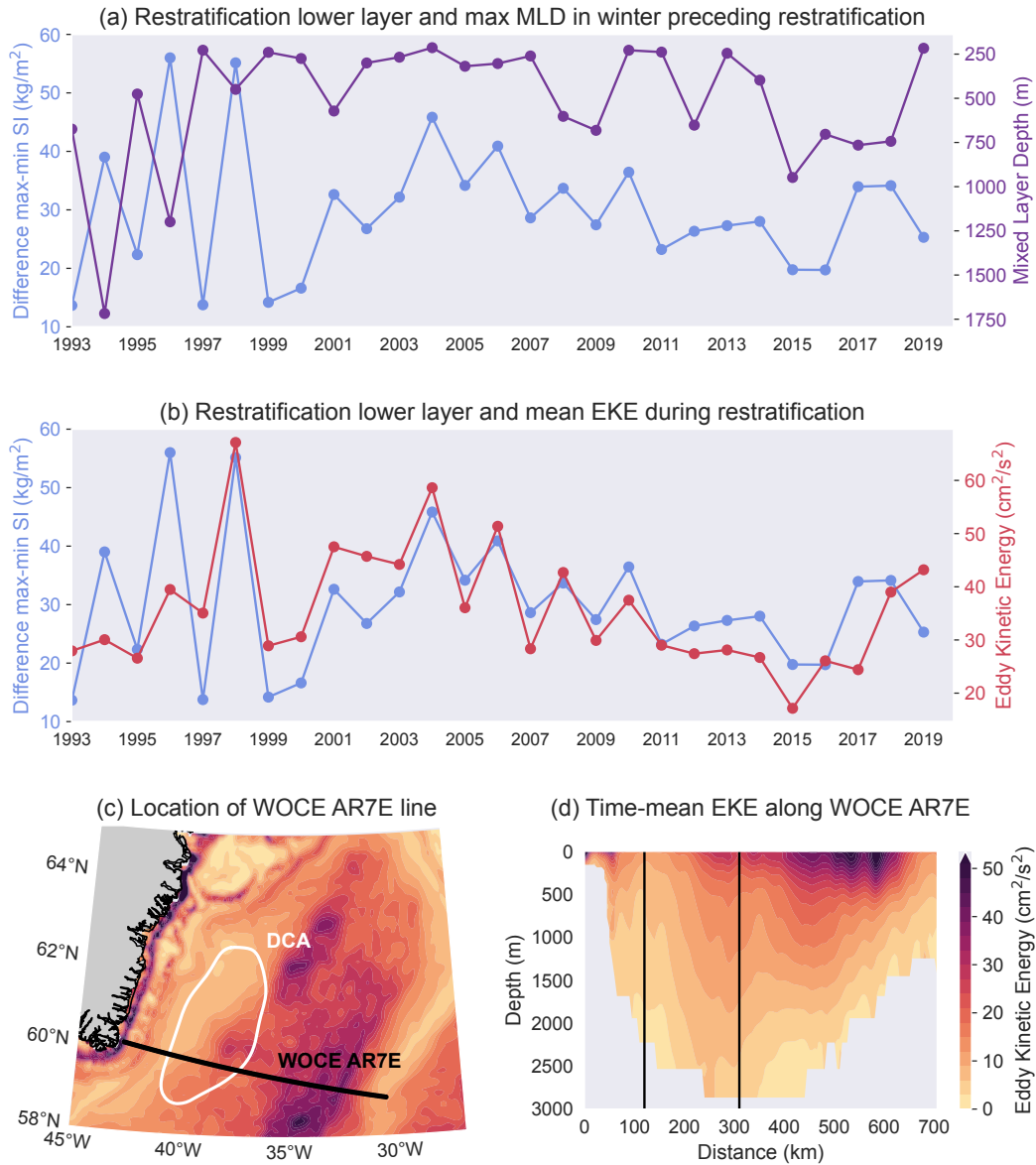


**Figure 9.** (a) Restratification and maximum mixed layer depth preceding the restatification period in the lower layer of the Deep Convection Area (DCA). (b) Restratification in the lower layer of the DCA and surface eddy kinetic energy (EKE) along the WOCE AR7E section eastward of the DCA, averaged over the restatification phase. The restatification period starts in the month after the occurrence of the minimum winter stratification and ends in the month of the next maximum stratification in the upper layer. (c) The WOCE AR7E line in the Irminger Sea (Koltermann et al., 2011) and the boundary of the DCA, plotted on top of the 1993–2019 mean EKE field averaged over the upper 600 m. (d) The 1993–2019 mean from the CMEMS reanalysis of the EKE along the WOCE AR7E line. The vertical black lines mark the points where the line intersects the DCA boundary.

346

The eddies from this region bring warm and saline Irminger Current water into the DCA

(Fan et al., 2013); this further supports the notion that eddies drive lower layer restratification.

## 4 Discussion and Conclusions

To summarise our results, most of the variability in stratification in the central Irminger Sea is located in the upper 600 m of the water column. We found distinctly different variability in stratification in the upper 100 m and the 100–600 m layer. In the upper layer, there is a strong seasonal cycle with freshening and warming in spring and summer and very little interannual variability. Exceptionally high upper layer stratification may be reached in years when both heat and freshwater fluxes are above average. In the lower layer, there is substantial interannual variability in stratification. The winter minimum stratification is determined by the strength of convection: deeper mixed layers lead to weaker stratification. The restratification after winter is strongly linked to the eddy kinetic energy in the eastern Irminger Sea, suggesting that warm, saline eddies shed by the Irminger Current play an important role in restratifying the DCA.

This two layer structure in restratification in the Irminger Sea is very similar to what is observed in the Labrador Sea (Straneo, 2006a), which also displays surface freshening during restratification while the layer below gets more saline. However, there is an important difference. At least part of the two layer structure of restratification in the Labrador Sea is derived from the two layer eddies shed from the boundary current. These eddies have a cold and fresh upper layer extending until 100 to 400 m depth and a warm and saline layer below (Lilly et al., 1999; Hátún et al., 2007; de Jong et al., 2014). However, in the Irminger Sea no eddies with a fresh top are observed, due to their origin in the Irminger Current which is warm and saline throughout (Fan et al., 2013). Instead, the upper layer freshening in the Irminger Sea is due to surface freshwater gain and thin layers of freshwater driven off the East Greenland shelf during strong wind events (Duyck et al., 2022).

Amplification of upper layer stratification through co-occurring above normal surface heat and freshwater gain was seen in 2010 and 2019. The 2010 event was described by Oltmanns et al. (2018). They speculate that the fresh surface layer might have had an additional continental origin. They found that surface temperatures were high in a broad area near the southeast Greenland shelf, where glacier melt would be accelerated. Freshening due to ice melt is a plausible cause for freshwater anomalies near the East Greenland shelf, which we know can be exported to the DCA (Foukal et al., 2020; Duyck & De Jong, 2021; Duyck et al., 2022) and thus increase the stratification there. In 2019 runoff from Greenland was high as well (Slater et al., 2021), but there was also an additional cause for the high stratification: a strong freshwater anomaly that formed between 2012 and 2016 in the eastern subpolar North Atlantic, as described by Holliday et al. (2020). This anomaly went on to propagate northwards into the Irminger Sea, the Labrador Sea and the Nordic Seas. Its effects can be seen in the freshening of the upper and intermediate layers in the Irminger Sea from 2017 onwards (Figure 3a) as well as in the high stratification in 2019 (Figure 6a). In the long term, anthropogenic climate change is expected to further enhance Greenland ice melt. Upper layer stratification increases as seen in 2010 and 2019 may occur more frequently and stronger.

The lower layer displays much stronger interannual variability, partly through longer ocean memory (set by convection in previous winters) and partly through differences in restratification. We found a strong relation between the strength of the annual restratification and the EKE in the eastern Irminger Sea. Anticyclonic eddies with warm and saline cores shed by the Irminger Current move westward into the DCA, thus restratifying it. In the Labrador Sea, eddies play a crucial role both in determining the location of the deep convection region (Chanut et al., 2008) as well as in the downwelling and export of convective waters (Georgiou et al., 2019). As the Irminger Sea is an im-

398 portant contributor to the overturning in the subpolar gyre (Lozier et al., 2019; Petit  
 399 et al., 2020; Li et al., 2021) it is imperative that eddy processes and their contribution  
 400 to restratification in the Irminger Sea are better understood.

## 401 Data Availability Statement

402 The CMEMS monthly mean data is available at [https://resources.marine.copernicus](https://resources.marine.copernicus.eu/product-detail/GLOBAL_MULTIYEAR_PHY_001_030/DATA-ACCESS)  
 403 [.eu/product-detail/GLOBAL\\_MULTIYEAR\\_PHY\\_001\\_030/DATA-ACCESS](https://resources.marine.copernicus.eu/product-detail/GLOBAL_MULTIYEAR_PHY_001_030/DATA-ACCESS). The files for 1993–  
 404 2012 were last accessed on 29-10-2020; the files for 2013–2019 were last accessed on 21-  
 405 05-2021.

406 The ERA5 monthly averaged data on single levels is available at [https://cds.climate](https://cds.climate.copernicus.eu/cdsapp#!/dataset/reanalysis-era5-single-levels-monthly-means?tab=overview)  
 407 [.copernicus.eu/cdsapp#!/dataset/reanalysis-era5-single-levels-monthly-means](https://cds.climate.copernicus.eu/cdsapp#!/dataset/reanalysis-era5-single-levels-monthly-means?tab=overview)  
 408 [?tab=overview](https://cds.climate.copernicus.eu/cdsapp#!/dataset/reanalysis-era5-single-levels-monthly-means?tab=overview) and was last accessed on 16-09-2021.

409 Data was processed using Python 3.6.13. All code used for processing data and mak-  
 410 ing figures for this study is available at <https://github.com/MiriamSterl/RestratificationIrmingerSea>.

## 411 Acknowledgments

412 This work was financially supported by the Innovational Research Incentives Scheme of  
 413 the Netherlands Organisation for Scientific Research (NWO) under grant agreement nos.  
 414 016.Vidi.189.130.

## 415 References

- 416 Bailey, D. A., Rhines, P. B., & Häkkinen, S. (2005). Formation and path-  
 417 ways of North Atlantic Deep Water in a coupled ice–ocean model of the  
 418 Arctic–North Atlantic Oceans. *Climate Dynamics*, *25*, 497–516. doi:  
 419 10.1007/s00382-005-0050-3
- 420 Brown, P. J., Mcdonagh, E. L., Sanders, R., Watson, A. J., King, B. A., Smeed,  
 421 D. A., ... Meinen, C. S. (2021). Anthropogenic carbon transports and up-  
 422 take. doi: 10.1038/s41561-021-00774-5
- 423 Chanut, J., Barñier, B., Large, W., Debreu, L., Penduff, T., Molines, J. M., & Math-  
 424 iot, P. (2008). Mesoscale eddies in the Labrador Sea and their contribution  
 425 to convection and restratification. *Journal of Physical Oceanography*, *38*,  
 426 1617–1643. doi: 10.1175/2008JPO3485.1
- 427 Cuny, J., Rhines, P. B., Niiler, P. P., & Bacon, S. (2002). Labrador Sea boundary  
 428 currents and the fate of the Irminger Sea Water. *Journal of Physical Oceanog-*  
 429 *raphy*, *32*, 627–647. doi: 10.1175/1520-0485(2002)032<0627:LSBCAT>2.0.CO;2
- 430 De Jong, M. F., Aken, H. M. V., Våge, K., & Pickart, R. S. (2012). Convective mix-  
 431 ing in the central Irminger Sea: 2002–2010. *Deep-Sea Research Part I: Oceanog-*  
 432 *raphic Research Papers*, *63*, 36–51. doi: 10.1016/j.dsr.2012.01.003
- 433 de Jong, M. F., Bower, A. S., & Furey, H. H. (2014). Two years of observations of  
 434 warm-core anticyclones in the Labrador Sea and their seasonal cycle in heat  
 435 and salt stratification. *Journal of Physical Oceanography*, *44*, 427–444. doi:  
 436 10.1175/JPO-D-13-070.1
- 437 de Jong, M. F., Bower, A. S., & Furey, H. H. (2016). Seasonal and interan-  
 438 nual variations of Irminger ring formation and boundary-interior heat ex-  
 439 change in FLAME. *Journal of Physical Oceanography*, *46*, 1717–1734. doi:  
 440 10.1175/JPO-D-15-0124.1
- 441 de Jong, M. F., & de Steur, L. (2016). Strong winter cooling over the Irminger  
 442 Sea in winter 2014–2015, exceptional deep convection, and the emergence of  
 443 anomalously low SST. *Geophysical Research Letters*, *43*, 7106–7113. doi:  
 444 10.1002/2016GL069596

- 446 de Jong, M. F., de Steur, L., Fried, N., Bol, R., & Kritsotakis, S. (2020). Year-  
 447 Round Measurements of the Irminger Current: Variability of a Two-Core  
 448 Current System Observed in 2014–2016. *Journal of Geophysical Research: Oceans*, *125*. doi: 10.1029/2020JC016193  
 449
- 450 de Jong, M. F., Oltmanns, M., Karstensen, J., & Society, T. O. (2018). Deep con-  
 451 vection in the Irminger Sea observed with a dense mooring array. *Oceanogra-  
 452 phy*, *31*, 50-59.
- 453 Dijkstra, H. A. (2008). *Dynamical oceanography*. Springer US. doi: 10.1007/978-3  
 454 -540-76376-5
- 455 Duyck, E., & De Jong, M. F. (2021). Circulation Over the South-East Greenland  
 456 Shelf and Potential for Liquid Freshwater Export: A Drifter Study. *Geophys-  
 457 ical Research Letters*, *48*, 1-9. doi: 10.1029/2020GL091948
- 458 Duyck, E., Gelderloos, R., & Jong, M. F. (2022, 5). Wind-Driven Freshwater Ex-  
 459 port at Cape Farewell. *Journal of Geophysical Research: Oceans*, *127*. doi: 10  
 460 .1029/2021jc018309
- 461 Fan, X., Send, U., Testor, P., Karstensen, J., & Lherminier, P. (2013). Observa-  
 462 tions of Irminger Sea anticyclonic eddies. *Journal of Physical Oceanography*,  
 463 *43*, 805-823. doi: 10.1175/JPO-D-11-0155.1
- 464 Fernandez, E., & Lellouche, J. M. (2018). Product User Manual For the Global  
 465 Ocean Physical Reanalysis product GLOBAL\_REANALYSIS\_PHY\_001\_030.
- 466 Foukal, N. P., Gelderloos, R., & Pickart, R. S. (2020). A continuous pathway for  
 467 fresh water along the East Greenland shelf. *Science Advances*, *6*. doi: 10.1126/  
 468 sciadv.abc4254
- 469 Fox-Kemper, B., Hewitt, H. T., Xiao, C., Adalgeirsdóttir, G., Drijfhout, S. S., Ed-  
 470 wards, T. L., ... Yu, Y. (2021). *Ocean, Cryosphere and Sea Level Change*.  
 471 Cambridge University Press. In Press.
- 472 Frajka-Williams, E., Rhines, P. B., & Eriksen, C. C. (2014). Horizontal stratifica-  
 473 tion during deep convection in the Labrador Sea. *Journal of Physical Oceanog-  
 474 raphy*, *44*, 220-228. doi: 10.1175/JPO-D-13-069.1
- 475 Fratantoni, D. M. (2001). North Atlantic surface circulation during the 1990's ob-  
 476 served with satellite-tracked drifters. *Journal of Geophysical Research*, *106*,  
 477 22,067-22,093.
- 478 Fried, N., & Jong, M. F. (2022, 3). The Role of the Irminger Current in the  
 479 Irminger Sea Northward Transport Variability. *Journal of Geophysical Re-  
 480 search: Oceans*, *127*. Retrieved from [https://onlinelibrary.wiley.com/  
 481 doi/10.1029/2021JC018188](https://onlinelibrary.wiley.com/doi/10.1029/2021JC018188) doi: 10.1029/2021JC018188
- 482 Fröb, F., Olsen, A., Våge, K., Moore, G. W., Yashayaev, I., Jeansson, E., & Ra-  
 483 jasakaren, B. (2016). Irminger Sea deep convection injects oxygen and an-  
 484 thropogenic carbon to the ocean interior. *Nature Communications*, *7*. doi:  
 485 10.1038/ncomms13244
- 486 Gelderloos, R., Katsman, C. A., & Drijfhout, S. S. (2011). Assessing the roles of  
 487 three eddy types in restratifying the Labrador Sea after deep convection. *Jour-  
 488 nal of Physical Oceanography*, *41*, 2102-2119. doi: 10.1175/JPO-D-11-054.1
- 489 Georgiou, S., van der Boog, C. G., Brüggemann, N., Ypma, S. L., Pietrzak, J. D., &  
 490 Katsman, C. A. (2019). On the interplay between downwelling, deep convec-  
 491 tion and mesoscale eddies in the Labrador Sea. *Ocean Modelling*, *135*, 56-70.  
 492 Retrieved from <https://doi.org/10.1016/j.ocemod.2019.02.004> doi:  
 493 10.1016/j.ocemod.2019.02.004
- 494 Herrmann, M., Sevault, F., Beuvier, J., & Somot, S. (2010). What induced the  
 495 exceptional 2005 convection event in the northwestern Mediterranean basin?  
 496 Answers from a modeling study. *Journal of Geophysical Research: Oceans*,  
 497 *115*, 1-19. doi: 10.1029/2010JC006162
- 498 Hersbach, H., Bell, B., Berrisford, P., Hirahara, S., Horányi, A., Muñoz-Sabater, J.,  
 499 ... Thépaut, J. N. (2020). The ERA5 global reanalysis. *Quarterly Journal of  
 500 the Royal Meteorological Society*, *146*, 1999-2049. doi: 10.1002/qj.3803

- 501 Holliday, N. P., Bersch, M., Berx, B., Chafik, L., Cunningham, S., Florindo-López,  
502 C., ... Yashayaev, I. (2020). Ocean circulation causes the largest freshening  
503 event for 120 years in eastern subpolar North Atlantic. *Nature Communica-*  
504 *tions*, 11. doi: 10.1038/s41467-020-14474-y
- 505 Hátún, H., Eriksen, C. C., & Rhines, P. B. (2007). Buoyant eddies entering  
506 the Labrador Sea observed with gliders and altimetry. *Journal of Physical*  
507 *Oceanography*, 37, 2838-2854. doi: 10.1175/2007JPO3567.1
- 508 Jones, H., & Marshall, J. (1997). Restratification after deep convection. *Journal of*  
509 *Physical Oceanography*, 27, 2276-2287. doi: 10.1175/1520-0485(1997)027<2276:  
510 RADC>2.0.CO;2
- 511 Katsman, C. A., Drijfhout, S. S., Dijkstra, H. A., & Spall, M. A. (2018). Sink-  
512 ing of dense North Atlantic waters in a global ocean model: Location and  
513 controls. *Journal of Geophysical Research: Oceans*, 123, 3563-3576. doi:  
514 10.1029/2017JC013329
- 515 Katsman, C. A., Spall, M. A., & Pickart, R. S. (2004). Boundary current eddies  
516 and their role in the restratification of the Labrador Sea. *Journal of Phys-*  
517 *ical Oceanography*, 34, 1967-1983. doi: 10.1175/1520-0485(2004)034<1967:  
518 BCEATR>2.0.CO;2
- 519 Koltermann, K., Gouretski, V., & Jancke, K. (2011). *Hydrographic Atlas of the*  
520 *World Ocean Circulation Experiment (WOCE), Volume 3: Atlantic Ocean*  
521 (J. G. M. Sparrow P. Chapman, Ed.).
- 522 Lazier, J., Hendry, R., Clarke, A., Yashayaev, I., & Rhines, P. (2002). Convection  
523 and restratification in the Labrador Sea, 1990-2000. *Deep-Sea Research Part I:*  
524 *Oceanographic Research Papers*, 49, 1819-1835. doi: 10.1016/S0967-0637(02)  
525 00064-X
- 526 Le Bras, I. A., Straneo, F., Holte, J., de Jong, M. F., & Holliday, N. P. (2020).  
527 Rapid Export of Waters Formed by Convection Near the Irminger Sea's West-  
528 ern Boundary. *Geophysical Research Letters*, 47. doi: 10.1029/2019GL085989
- 529 Le Bras, I. A., Straneo, F., Holte, J., & Holliday, N. P. (2018). Seasonality of Fresh-  
530 water in the East Greenland Current System From 2014 to 2016. *Journal of*  
531 *Geophysical Research: Oceans*, 123, 8828-8848. doi: 10.1029/2018JC014511
- 532 L'Hévéder, B., Li, L., Sevault, F., & Somot, S. (2013). Interannual variability of  
533 deep convection in the Northwestern Mediterranean simulated with a coupled  
534 AORCM. *Climate Dynamics*, 41, 937-960. doi: 10.1007/s00382-012-1527-5
- 535 Li, F., Lozier, M. S., Holliday, N. P., Johns, W. E., Le Bras, I. A., Moat, B. I., ...  
536 de Jong, M. F. (2021). Observation-based estimates of heat and freshwa-  
537 ter exchanges from the subtropical North Atlantic to the Arctic. *Progress*  
538 *in Oceanography*, 197, 102640. Retrieved from [https://doi.org/10.1016/  
539 j.pocean.2021.102640](https://doi.org/10.1016/j.pocean.2021.102640) doi: 10.1016/j.pocean.2021.102640
- 540 Lilly, J. M., Rhines, P. B., Visbeck, M., Davis, R., Lazier, J. R., Schott, F., &  
541 Farmer, D. (1999). Observing deep convection in the Labrador Sea dur-  
542 ing winter 1994/95. *Journal of Physical Oceanography*, 29, 2065-2098. doi:  
543 10.1175/1520-0485(1999)029<2065:odciti>2.0.co;2
- 544 Lozier, M. S., Li, F., Bacon, S., Bahr, F., Bower, A. S., Cunningham, S. A., ...  
545 Zhao, J. (2019). A sea change in our view of overturning in the subpolar North  
546 Atlantic. *Science*, 363, 516-521. doi: 10.1126/science.aau6592
- 547 Madec, G. (2016). *NEMO Ocean Engine*. Retrieved from [http://www.nemo-ocean  
548 .eu/About-NEMO/Reference-manuals%5Cnpapers2://publication/uuid/  
549 73E7FF17-99BE-4B10-A823-0037C823EF6E](http://www.nemo-ocean.eu/About-NEMO/Reference-manuals%5Cnpapers2://publication/uuid/73E7FF17-99BE-4B10-A823-0037C823EF6E) doi: 10.5281/zenodo.3248739
- 550 Margirier, F., Testor, P., Heslop, E., Mallil, K., Bosse, A., Houpert, L., ... Tail-  
551 landier, V. (2020). Abrupt warming and salinification of intermediate waters  
552 interplays with decline of deep convection in the Northwestern Mediterranean  
553 Sea. *Scientific Reports*, 10, 1-11. Retrieved from [https://doi.org/10.1038/  
554 s41598-020-77859-5](https://doi.org/10.1038/s41598-020-77859-5) doi: 10.1038/s41598-020-77859-5

- 555 Marshall, J., & Schott, F. (1999). Open-Ocean Convection: Observations, Theory,  
556 and Models. *Reviews of Geophysics*, *37*, 1-64.
- 557 McCarthy, G. D., Smeed, D. A., Cunningham, S. A., & Roberts, C. D. (2017). At-  
558 lantic Meridonal Overturning Circulation. *Marine Climate Change Impacts*  
559 *Partnership: Science Review*, 15-21. Retrieved from [www.ncdc.noaa.gov](http://www.ncdc.noaa.gov).  
560 doi: 10.14465/2017.arc10.002-atl
- 561 McDougall, T. J., & Barker, P. (2011). *Getting started with TEOS-10 and the Gibbs*  
562 *Seawater (GSW) Oceanographic Toolbox*. SCOR/IAPSO WG127. Retrieved  
563 from [http://www.teos-10.org/pubs/gsw/v3\\_04/pdf/Getting\\_Started.pdf](http://www.teos-10.org/pubs/gsw/v3_04/pdf/Getting_Started.pdf)
- 564 Oltmanns, M., Karstensen, J., & Fischer, J. (2018). Increased risk of a shutdown  
565 of ocean convection posed by warm North Atlantic summers. *Nature Cli-*  
566 *mate Change*, *8*, 300-304. Retrieved from [http://dx.doi.org/10.1038/](http://dx.doi.org/10.1038/s41558-018-0105-1)  
567 [s41558-018-0105-1](http://dx.doi.org/10.1038/s41558-018-0105-1) doi: 10.1038/s41558-018-0105-1
- 568 Petit, T., Lozier, M. S., Josey, S. A., & Cunningham, S. A. (2020). Atlantic Deep  
569 Water Formation Occurs Primarily in the Iceland Basin and Irminger Sea  
570 by Local Buoyancy Forcing. *Geophysical Research Letters*, *47*, 1-9. doi:  
571 10.1029/2020GL091028
- 572 Pickart, R. S., Straneo, F., & Moore, G. W. (2003). Is Labrador Sea Water formed  
573 in the Irminger basin? *Deep-Sea Research Part I: Oceanographic Research Pa-*  
574 *pers*, *50*, 23-52. doi: 10.1016/S0967-0637(02)00134-6
- 575 Piron, A., Thierry, V., Mercier, H., & Caniaux, G. (2016). Argo float observations  
576 of basin-scale deep convection in the Irminger sea during winter 2011–2012.  
577 *Deep-Sea Research Part I: Oceanographic Research Papers*, *109*, 76-90.  
578 Retrieved from <http://dx.doi.org/10.1016/j.dsr.2015.12.012> doi:  
579 10.1016/j.dsr.2015.12.012
- 580 Pérez, F. F., Mercier, H., Vázquez-Rodríguez, M., Lherminier, P., Velo, A., Pardo,  
581 P. C., ... Ríos, A. F. (2013). Atlantic Ocean CO<sub>2</sub> uptake reduced by weaken-  
582 ing of the meridional overturning circulation. *Nature Geoscience*, *6*, 146-152.  
583 doi: 10.1038/ngeo1680
- 584 Sampe, T., & Xie, S. P. (2007). Mapping high sea winds from space: A global clima-  
585 tology. *Bulletin of the American Meteorological Society*, *88*, 1965-1978. doi: 10  
586 .1175/BAMS-88-12-1965
- 587 Slater, T., Shepherd, A., McMillan, M., Leeson, A., Gilbert, L., Muir, A., ... Briggs,  
588 K. (2021, 12). Increased variability in Greenland Ice Sheet runoff from satellite  
589 observations. *Nature Communications*, *12*. doi: 10.1038/s41467-021-26229-4
- 590 Somot, S., Houpert, L., Sevault, F., Testor, P., Bosse, A., Taupier-Letage, I.,  
591 ... Herrmann, M. (2018). Characterizing, modelling and understand-  
592 ing the climate variability of the deep water formation in the North-  
593 Western Mediterranean Sea. *Climate Dynamics*, *51*, 1179-1210. doi:  
594 10.1007/s00382-016-3295-0
- 595 Straneo, F. (2006a). Heat and freshwater transport through the central Labrador  
596 Sea. *Journal of Physical Oceanography*, *36*, 606-628. doi: 10.1175/JPO2875.1
- 597 Straneo, F. (2006b). On the connection between dense water formation, overturn-  
598 ing, and poleward heat transport in a convective basin. *Journal of Physical*  
599 *Oceanography*, *36*, 1822-1840. doi: 10.1175/JPO2932.1
- 600 Volkov, D. L. (2005). Interannual variability of the altimetry-derived eddy field  
601 and surface circulation in the extratropical North Atlantic Ocean in 1993-2001.  
602 *Journal of Physical Oceanography*, *35*, 405-426. doi: 10.1175/JPO2683.1
- 603 Våge, K., Pickart, R. S., Sarafanov, A., Øyvind Knutsen, Mercier, H., Lherminier,  
604 P., ... Bacon, S. (2011). The Irminger Gyre: Circulation, convection, and  
605 interannual variability. *Deep-Sea Research Part I: Oceanographic Research*  
606 *Papers*, *58*, 590-614. doi: 10.1016/j.dsr.2011.03.001
- 607 Yashayaev, I., & Loder, J. W. (2017). Further intensification of deep convection in  
608 the Labrador Sea in 2016. *Geophysical Research Letters*, *44*, 1429-1438. doi: 10  
609 .1002/2016GL071668

# Supporting Information for ”Restratification Structure and Processes in the Irminger Sea”

M. F. Sterl<sup>1,2</sup> and M. F. de Jong<sup>1</sup>

<sup>1</sup>Department of Ocean Systems, NIOZ, Royal Netherlands Institute for Sea Research, Texel, The Netherlands

<sup>2</sup>Institute for Marine and Atmospheric Research, Utrecht University, Utrecht, The Netherlands

## Contents of this file

1. Figure S1

## Introduction

To validate the time series from the CMEMS reanalysis, we compare them with time series from the LOCO mooring in Figure S1. Values of all properties are very similar in the CMEMS and LOCO time series. In both time series, the salinity has a mid-depth minimum, whereas the temperature and density have monotonously stratified structures. The MLD follows the same temporal trends in both data sets, with local maxima in 2008, 2009 and 2015 observable in both time series. Also, features of individual years such as the salinity and density maximum in the 2010–2011 winter are visible in both the CMEMS and the LOCO data. Thus, we conclude that the CMEMS reanalysis accurately captures the interannual variability of hydrographic properties in the Irminger Sea.

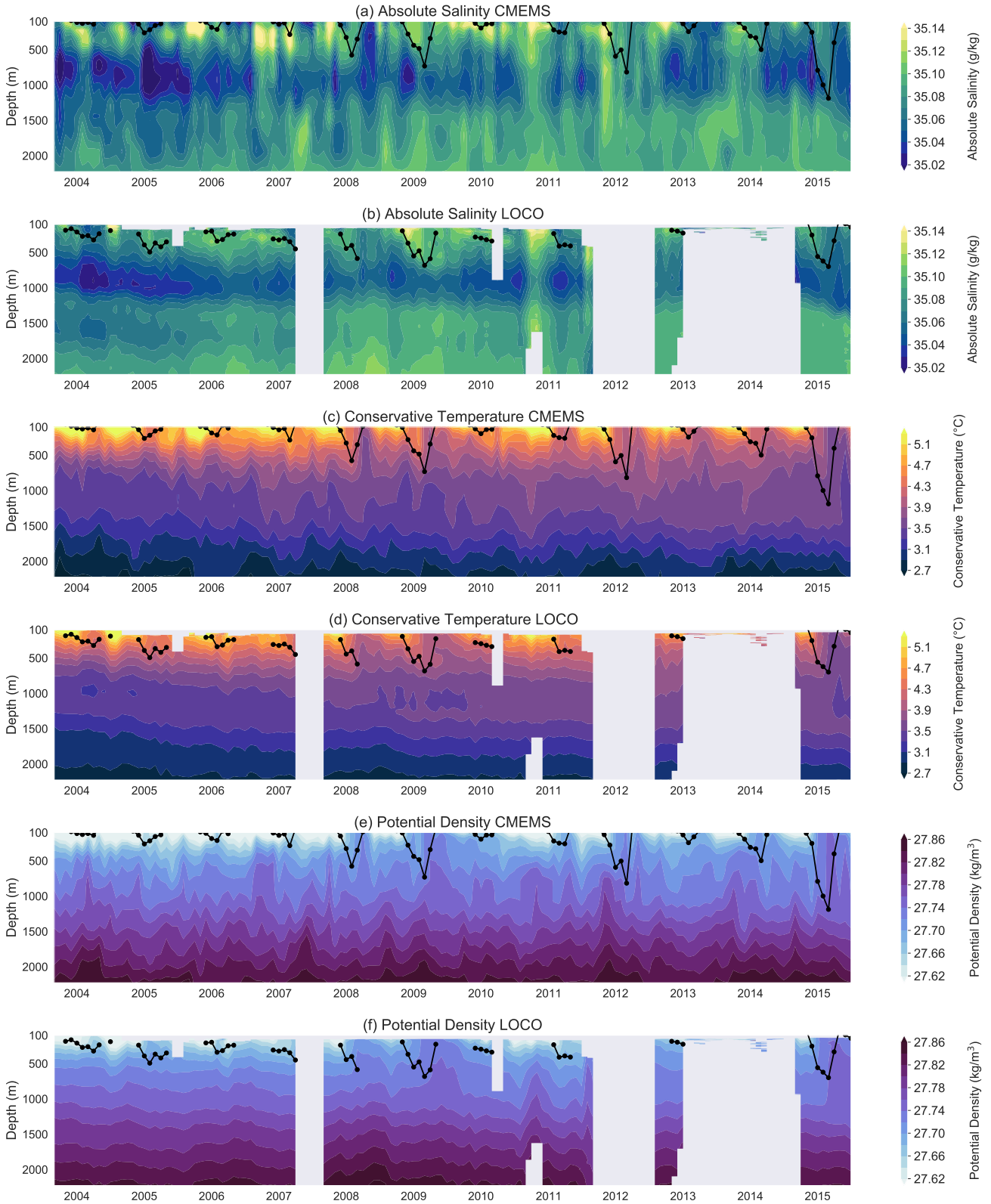


**Figure S1.** The temporal evolution of profiles of (a)-(b) absolute salinity, (c)-(d) conservative temperature and (e)-(f) potential density at the LOCO mooring. The mixed layer depth is shown in black. Panels (a), (c) and (e) show the data from the CMEMS reanalysis interpolated to the mooring location. Panels (b), (d) and (f) show the data from the LOCO mooring.

July 15, 2022, 8:45am